

# Abelian and non-Abelian gauge fields in dipole-dipole interacting Rydberg atoms

Martin Kiffner<sup>1,2</sup>, Wenhui Li<sup>1,3</sup>, and Dieter Jaksch<sup>2,1</sup>

*Centre for Quantum Technologies, National University of Singapore, 3 Science Drive 2, Singapore 117543<sup>1</sup>  
Clarendon Laboratory, University of Oxford, Parks Road, Oxford OX1 3PU, United Kingdom<sup>2</sup> and  
Department of Physics, National University of Singapore, 117542, Singapore<sup>3</sup>*

We show that the dipole-dipole interaction between two Rydberg atoms can lead to substantial Abelian and non-Abelian gauge fields acting on the relative motion of the two atoms. We demonstrate how the gauge fields can be evaluated by numerical techniques. In the case of adiabatic motion in a single internal state, we show that the gauge fields give rise to a magnetic field that results in a Zeeman splitting of the rotational states. In particular, the ground state of a molecular potential well is given by the first excited rotational state. We find that our system realises a synthetic spin-orbit coupling where the relative atomic motion couples to two internal two-atom states. The associated gauge fields are non-Abelian.

PACS numbers: 03.65.Vf, 03.75.-b, 32.80.Rm

## I. INTRODUCTION

Gauge theories are of fundamental importance in modern theoretical physics. Examples are given by classical and quantum electrodynamics and the standard model of elementary particle physics. In addition, it has been realised that Abelian and non-Abelian gauge fields arise in the adiabatic evolution of quantum mechanical systems [1]. This concept was applied to molecules in [2], where the realisation of magnetic monopoles is discussed. However, the simulation of gauge fields with conventional molecules is impractical for several reasons. First, the gauge fields arise from those terms that are usually neglected in the ubiquitous Born-Oppenheimer (BO) approximation [3]. Since the BO approximation is very well satisfied in many systems due to the huge mass difference between electrons and nuclei, the desired gauge field effects are usually very small. Second, the experimental observation is considerably hampered by the small size of conventional molecules. Third, not all gauge fields give rise to magnetic fields, and it is very challenging to engineer non-trivial gauge fields via external manipulations of the electronic levels. For these reasons, other systems for the simulation of artificial gauge fields have been explored. In particular, tremendous experimental and theoretical effort has been made to simulate gauge fields with cold atoms [4–15] in tailored electromagnetic fields.

The exaggerated properties of Rydberg atoms [16] give rise to various exceptional phenomena in quantum optics [17] and quantum information science [18]. For example, it is possible to form exotic molecules that are orders of magnitude larger than naturally occurring molecules. So-called trilobite molecules are comprised of one Rydberg atom and one ground state atom, where the bond is mediated by the interaction of the Rydberg electron with the ground state atom [19, 20]. On the other hand, Rydberg macrodimers consist of two Rydberg atoms with non-overlapping electron clouds [21–24], and the binding potential arises from the dipole-dipole interaction. Since typical internuclear spacings exceed  $1 \mu\text{m}$ , the experimen-

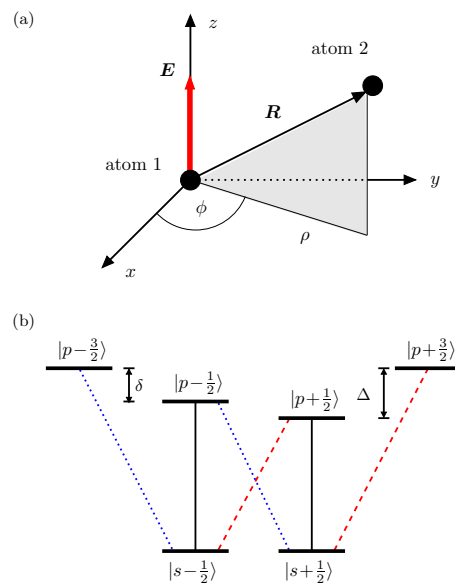


FIG. 1. (Color online) (a) The system under consideration consists of two Rydberg atoms.  $\mathbf{R}$  is the relative position of atom 2 with respect to atom 1. An external electric field  $\mathbf{E}$  is applied in the  $z$  direction.  $\rho$  is the distance of atom 2 from the  $z$  axis. (b) Internal level structure of each Rydberg atom. The Stark shifts  $\delta \equiv W_{p-1/2} - W_{p-3/2}$  and  $\Delta \equiv W_{p+1/2} - W_{p+3/2}$  are negative. We assume  $\delta \neq \Delta$ . The dipole transitions indicated by solid, blue dotted and red dashed lines couple to  $\pi$ ,  $\sigma^-$  and  $\sigma^+$  polarised fields, respectively.

tal observation of Rydberg-Rydberg correlations becomes feasible [25]. Moreover, several features like the internuclear spacing and the angular dependence of the binding potential can be controlled in some Rydberg macrodimer schemes.

Here we show that the dipole-dipole interaction between two Rydberg atoms gives rise to sizeable Abelian and non-Abelian gauge fields acting on the relative motion of the two atoms. Our system is several orders of magnitude larger than conventional molecules, and non-trivial gauge fields can be engineered via the exquisite

ability to manipulate and control individual Rydberg atoms. More specifically, our system shown in Fig. 1 is based on the Rydberg macrodimer proposal in [23], but here we consider an asymmetric Stark shift which breaks the symmetry of the system. Furthermore, it involves only a relatively small number of atomic states which facilitates the calculation of artificial gauge fields. We show that the dipole-dipole interaction gives rise to an artificial magnetic field for adiabatic motion in a donut-shaped potential well. This magnetic field results in a Zeeman shift of rotational states. In particular, the molecular ground state is given by the first excited rotational state. Furthermore, we show that the gauge fields can induce non-adiabatic transitions near an avoided crossing where two internal states become near-degenerate. Our system thus realises a synthetic spin-orbit coupling, and the associated gauge fields are strongly non-Abelian.

This paper is organised as follows. We give a detailed description of our system and the theoretical framework of artificial gauge fields in Sec. II. Some details are deferred to Appendix A. In Sec. III we assume that the relative atomic motion is confined to a donut-shaped potential well and evaluate the corresponding Abelian vector potential. We find that it gives rise to a position-dependent magnetic field and calculate the first excited bound states of the potential well. In Sec. IV we show that the relative atomic motion can induce non-adiabatic transitions between two internal states exhibiting an avoided crossing. With the techniques described in Appendices B and C we evaluate the corresponding gauge fields and show that they are non-Abelian. Finally, we conclude with a summary and outlook in Sec. V.

## II. MODEL

The geometry of the two atom system under consideration is shown in Fig. 1a. The vector  $\mathbf{R}$  is the relative position of atom 2 with respect to atom 1. We are interested in the relative motion of the two Rydberg atoms that are coupled via the dipole-dipole interaction. The total Hamiltonian for the relative motion of the two atoms and the internal states is

$$H = H_{\text{R}} + H_{\text{int}}, \quad (1)$$

where

$$H_{\text{R}} = \frac{\mathbf{p}^2}{2\mu} \quad (2)$$

is the kinetic energy of the relative motion and  $\mu$  is the reduced mass of the two Rydberg atoms. We omit the centre-of-mass motion which is uniform. The Hamiltonian describing the internal degrees of freedom is given by

$$H_{\text{int}} = H_{\text{S}} + V_{\text{dd}}, \quad (3)$$

where  $H_{\text{S}}$  describes the internal levels of the two uncoupled atoms and  $V_{\text{dd}}$  is the dipole-dipole interaction (for

details see Appendix A). In each Rydberg atom we consider two angular momentum multiplets. The lower  $ns_{1/2}$  states have total angular momentum  $J = 1/2$ , and the excited multiplet is comprised of  $np_{3/2}$  states with total angular momentum  $J = 3/2$ . We specify the individual atomic states by their orbital angular momentum  $\ell$  and azimuthal total angular momentum  $m_j$ , i. e. as  $|\ell m_j\rangle$ . A DC electric field  $\mathbf{E}$  in the  $z$  direction defines the quantisation axis and gives rise to Stark shifts of the magnetic sublevels. We assume that the Stark shifts are different in the  $m_j > 0$  and  $m_j < 0$  manifolds, which could be achieved by inducing additional AC stark shifts, see Appendix A. For simplicity we focus on the level scheme shown in Fig. 1(b), where the asymmetry is characterised by a single parameter  $\Delta/\delta$  with  $\delta \equiv W_{p-1/2} - W_{p-3/2}$  and  $\Delta \equiv W_{p+1/2} - W_{p+3/2}$ . The total internal state space of the two atoms is spanned by 36 states. Here we focus on the subspace spanned by the  $nsnp$  states where one atom is in a  $ns_{1/2}$  state and the other in a  $np_{3/2}$  state. This subspace has dimension  $N = 16$  and is spanned by two sets of 8 basis states given by  $|sm_{1/2}, pm_{3/2}\rangle$  and  $|pm_{3/2}, sm_{1/2}\rangle$ . It is convenient to classify these two-atom states with respect to the total azimuthal angular momentum  $M$ . There are eight states with  $|M| = 1$ , four with  $M = 0$  and four with  $|M| = 2$ . The  $nsnp$  states are eigenstates of the Hamiltonian  $H_{\text{S}}$ , but not of the dipole-dipole interaction  $V_{\text{dd}}$ . Since the dipole-dipole interaction depends on the magnitude and orientation of the separation vector  $\mathbf{R}$ , the eigenstates and eigenvalues of  $H_{\text{int}}$  will depend on  $\mathbf{R}$ , too. In order to account for the azimuthal symmetry of the system, we express  $\mathbf{R}$  in terms of cylindrical coordinates,

$$\mathbf{R} = (\rho \cos \phi, \rho \sin \phi, z). \quad (4)$$

For every value of  $\mathbf{R}$  we introduce a set of orthonormal eigenstates of the Hamiltonian  $H_{\text{int}}$ ,

$$H_{\text{int}}|\psi_i(\mathbf{R})\rangle = \epsilon_i(\mathbf{R})|\psi_i(\mathbf{R})\rangle, \quad (5)$$

where  $\epsilon_i(\mathbf{R})$  are the corresponding eigenvalues. Due to the azimuthal symmetry of the problem, the eigenvalues depend only on  $z$  and  $\rho$ , but not on  $\phi$  [26]. The full quantum state of the two-atom system is thus described by the state vector

$$|\Psi\rangle = \sum_{i=1}^N \int d^3R \alpha_i(\mathbf{R}) |\psi_i(\mathbf{R})\rangle \otimes |\mathbf{R}\rangle, \quad (6)$$

where the sum runs over the  $N = 16$  eigenstates of the  $nsnp$  subspace. We follow the procedure described in [4–6] and derive from Eqs. (3) and (6) an effective Schrödinger equation for the wavefunctions  $\boldsymbol{\alpha} = (\alpha_1, \dots, \alpha_N)$ . We obtain

$$i\hbar\partial_t \boldsymbol{\alpha} = \left[ \frac{1}{2\mu} (\mathbf{p}\mathbf{1} - \mathbf{A})^2 + V \right] \boldsymbol{\alpha}, \quad (7)$$

where  $V$  and  $\mathbf{A}$  are  $N \times N$  matrices that are defined as

$$V_{kl} = \delta_{kl} \epsilon_k(\mathbf{R}), \quad (8)$$

$$\mathbf{A}_{kl} = i\hbar \langle \psi_k(\mathbf{R}) | \nabla | \psi_l(\mathbf{R}) \rangle, \quad (9)$$

and  $\delta_{kl}$  is the Kronecker delta. Note that each matrix element  $\mathbf{A}_{kl}$  is a 3-column vector. In the following,  $A^{(s)}$  denotes the matrix comprised of matrix elements  $A_{nm}^{(s)} = \mathbf{A}_{nm} \cdot \mathbf{e}_s$ , where  $\mathbf{e}_s$  is a 3-column unit vector and the dot denotes the (real) scalar product. We use  $s \in \{1, 2, 3\}$  for the Cartesian unit vectors as well as  $s \in \{\rho, z, \phi\}$  with

$$\mathbf{e}_\rho = \cos \phi \mathbf{e}_1 + \sin \phi \mathbf{e}_2, \quad \mathbf{e}_z = \mathbf{e}_3, \quad (10)$$

$$\mathbf{e}_\phi = -\sin \phi \mathbf{e}_1 + \cos \phi \mathbf{e}_2. \quad (11)$$

The same notation convention applies to other objects of the same structure as  $\mathbf{A}$ .

The off-diagonal terms  $|\mathbf{A}_{kl}|$  ( $k \neq l$ ) can induce transitions between two potential curves  $k$  and  $l$ , depending on the energy difference  $|\epsilon_k - \epsilon_l|$  and the velocity of the relative motion (see Sec. IV). Here we assume that the relative motion is confined to the first  $q$  eigenstates of  $H_{\text{int}}$ , i.e., there may be non-adiabatic transitions within the first  $q$  eigenstates, but transitions to other states  $|\psi_l(\mathbf{R})\rangle$  ( $l > q$ ) can be neglected. In this case, projection of Eq. (7) onto the relevant levels  $\tilde{\alpha} = (\alpha_1, \dots, \alpha_q)$ ,  $q < N$ , results in the following Schrödinger equation for  $\tilde{\alpha}$  [4–6],

$$i\hbar\partial_t\tilde{\alpha} = \left[ \frac{1}{2\mu}(\mathbf{p}\mathbb{1} - \tilde{\mathbf{A}})^2 + \tilde{V} + \Phi \right] \tilde{\alpha}. \quad (12)$$

Here  $\tilde{V}$  and  $\tilde{\mathbf{A}}$  are  $q \times q$  matrices whose matrix elements for  $k, l \leq q$  are given by Eqs. (8) and (9), respectively. The scalar potential results from the remaining states outside the considered subspace and is defined as

$$\Phi_{kl} = \frac{1}{2\mu} \sum_{p=q+1}^N \mathbf{A}_{kp} \cdot \mathbf{A}_{pl}. \quad (13)$$

The fields  $\tilde{\mathbf{A}}$  and  $\Phi$  transform under a basis change

$$\tilde{\alpha} \rightarrow U(\mathbf{R})\tilde{\alpha} \quad (14)$$

according to

$$\tilde{\mathbf{A}} \rightarrow U(\mathbf{R})\tilde{\mathbf{A}}U^\dagger(\mathbf{R}) - i\hbar[\nabla U(\mathbf{R})]U^\dagger(\mathbf{R}), \quad (15)$$

$$\Phi \rightarrow U(\mathbf{R})\Phi U^\dagger(\mathbf{R}). \quad (16)$$

It follows that  $\mathbf{A}$  and  $\Phi$  can be regarded as gauge fields. The vector potential gives rise to an effective magnetic field  $\mathbf{B}$  whose Cartesian components  $B^{(i)}$  ( $i \in \{1, 2, 3\}$ ) are defined as

$$B^{(i)} = \frac{1}{2}\varepsilon_{ikl}F^{(kl)}, \quad (17)$$

$$F^{(kl)} = \Omega^{(kl)} - \frac{i}{\hbar} \left[ \tilde{A}^{(k)}, \tilde{A}^{(l)} \right], \quad (18)$$

where we employed Einstein's sum convention,  $\varepsilon_{ikl}$  is the Levi-Civita tensor and

$$\Omega^{(kl)} = \partial_k \tilde{A}^{(l)} - \partial_l \tilde{A}^{(k)} \quad (19)$$

is the Berry curvature. Note that the last term in Eq. (18) is different from zero if the  $q \times q$  matrices  $\tilde{A}^{(k)}$  do not

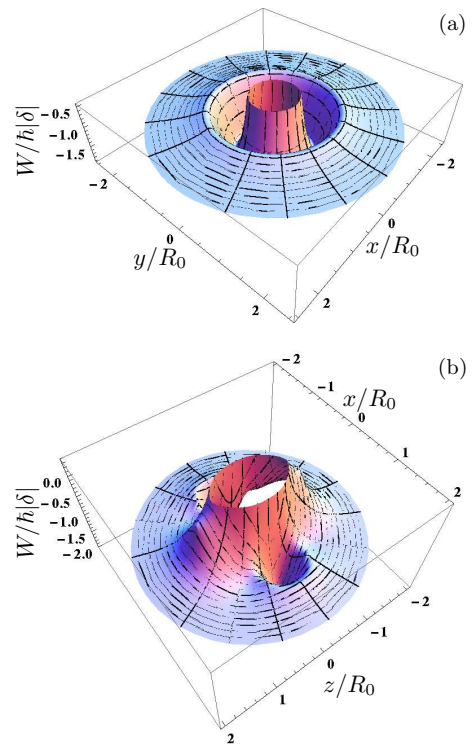


FIG. 2. (Color online) (a) Potential curve of the well state in the  $x - y$  plane. The potential is azimuthally symmetric around the  $z$  axis, giving rise to a donut-shaped potential well. (b) Potential curve of the well state in the  $x - z$  plane. Two pronounced minima occur on the  $\pm x$  axes. In (a) and (b) we set  $\Delta = -3|\delta|$ .

commute. In this case, the gauge fields are called non-Abelian.

In summary, the Hamiltonian in Eq. (12) is equivalent to the minimal coupling Hamiltonian of a charged particle in an electromagnetic field, characterised by the vector potential  $\tilde{\mathbf{A}}$  and scalar potential  $\Phi$ . We point out that the charge of the fictitious particle with mass  $\mu$  does not appear explicitly in Eq. (12). All fields  $\tilde{\mathbf{A}}$ ,  $\mathbf{B}$  and  $\Phi$  represent a charge multiplied with the corresponding field. In our framework it is impossible to determine the value of the charge by auxiliary measurements, and hence its value is arbitrary.

### III. ABELIAN GAUGE FIELD

Here we consider the adiabatic motion in a single eigenstate  $|\psi_1\rangle$  of  $H_{\text{int}}$  with energy  $\epsilon_1$ , see Eq. (5). Since this scenario corresponds to  $q = 1$  in Eq. (12), the Cartesian components of the vector potential are numbers and thus represent an Abelian gauge field. It was shown in [23] that the two dipole-dipole interacting Rydberg atoms exhibit a donut shaped potential well in the  $x - y$  plane for  $\delta = \Delta < 0$ . We find that this potential well persists in the case of an asymmetric Stark splitting  $\delta \neq \Delta$  and

denote the corresponding eigenstate and potential curve by  $|\psi_w\rangle$  and  $\epsilon_w$ , respectively. In the following we set  $|\psi_1\rangle = |\psi_w\rangle$ ,  $\epsilon_1 = \epsilon_w$  and investigate the vector potential, the corresponding magnetic field and the spectrum of the Hamiltonian in Eq. (12).

We begin with a characterisation of the potential well for  $\delta \neq \Delta$ . Due to the azimuthal symmetry of the system, a donut shaped potential well arises in the  $x-y$  plane [see Fig. 2(a)]. The spatial extend of the trapping potential in the  $x-z$  plane is shown in Fig. 2(b). The angular width of the potential around the  $x$  axis is about  $\pm 20^\circ$ , which is similar to the case  $\delta = \Delta$  studied in [23]. The depth of the potential increases with decreasing ratio  $\delta/\Delta$  of the detunings as shown in Fig. 3(a). If the separation vector  $\mathbf{R}$  lies in the  $x-y$  plane, the well state  $|\psi_w\rangle$  is contained within the  $M = \pm 1$  manifold and its corresponding potential curve  $\epsilon_w$  converges to the  $-\hbar|\delta|$  asymptote for  $R \rightarrow \infty$ . The potential minimum occurs roughly at  $R_0$  [see Eq. (A5)], which denotes the distance where the magnitude of the dipole-dipole interaction equals the Stark splitting  $\hbar|\delta|$ .

Next we investigate the vector potential arising from the adiabatic motion in the well state  $|\psi_w\rangle$ ,

$$\mathbf{A}_w = i\hbar\langle\psi_w|\nabla|\psi_w\rangle. \quad (20)$$

We find (see Appendix B) that the only non-zero component is given by

$$A_w^{(\phi)}(\rho, z) = \frac{1}{\rho}\langle\psi_w(\mathbf{R})|J_z|\psi_w(\mathbf{R})\rangle, \quad (21)$$

where  $J_z = J_z^{(1)} + J_z^{(2)}$  and  $J_z^{(\mu)}$  is the  $z$  component of the total angular momentum operator of the internal states of atom  $\mu$ . Note that  $A_w^{(\phi)}(\rho, z)$  does not depend on  $\phi$  because of the azimuthal symmetry of the system. It follows that  $\mathbf{A}_w$  obeys the Coulomb gauge ( $\text{div}\mathbf{A}_w = 0$ ) as a result of the phase convention described in Appendix B. The magnetic field  $\mathbf{B} = \nabla \times \mathbf{A}_w$  in Eq. (17) is given by

$$\mathbf{B} = \frac{1}{\rho} \left[ -\partial_z(\rho A_w^{(\phi)})\mathbf{e}_\rho + \partial_\rho(\rho A_w^{(\phi)})\mathbf{e}_z \right]. \quad (22)$$

Note that  $\mathbf{B}$  can be also calculated independently of  $A_w^{(\phi)}$  as shown in Appendix C. If the atoms are aligned in the  $x-y$  plane, we find that only the component  $B^{(3)}$  is different from zero. Figure 3(b) shows  $B^{(3)}$  for different ratios  $\delta/\Delta$ .

We emphasise that the magnetic field is only different from zero if we break the symmetry in the system, i.e., for  $\delta \neq \Delta$ . In order to understand this result, we write the well state as

$$|\psi_w\rangle = \sum_{M=-2}^2 a_M |p_M\rangle, \quad (23)$$

where  $|p_M\rangle$  is the normalised projection of  $|\psi_w\rangle$  onto the subspace with total angular momentum  $M$ . We thus have

$$\langle\psi_w|J_z|\psi_w\rangle = \hbar \sum_{M=-2}^2 M |a_M|^2, \quad (24)$$

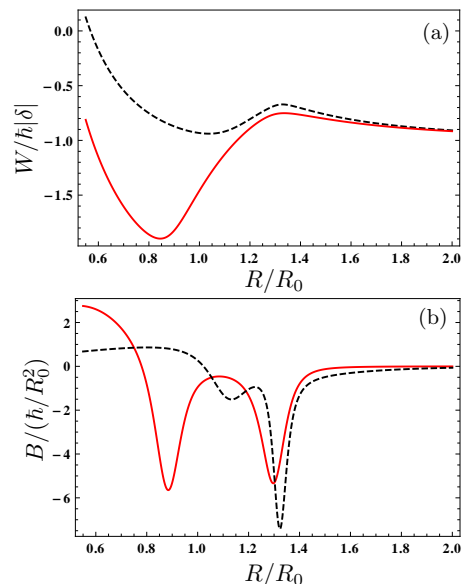


FIG. 3. (Color online) (a) Potential curve  $\epsilon_w$  of the well state in the  $x-y$  plane as a function of scaled internuclear spacing  $R/R_0$ . (b) The  $z$  component of the artificial magnetic field for  $\mathbf{R}$  in the  $x-y$  plane. In this spatial configuration, the  $x$  and  $y$  components of  $\mathbf{B}$  are zero. The parameters in (a)-(b) are  $\Delta = -3|\delta|$  (solid red line) and  $\Delta = -1.3|\delta|$  (black dashed line).

and hence Eq. (21) implies that  $A^{(\phi)}(\rho, z)$  will be zero if the level scheme is symmetric: In this case,  $|\psi_w\rangle$  resides equally in states with positive and negative values of  $M$ , i.e.,  $|a_M| = |a_{-M}|$ . Conversely, a broken symmetry will give rise to a non-trivial vector potential since the population of  $|\psi_w\rangle$  will be distributed unevenly over the  $\pm M$  subspaces.

The quantum dynamics of the relative atomic motion is governed by Eq. (12). The corresponding Hamiltonian is given by

$$H_w = \frac{1}{2\mu}(\mathbf{p} - \mathbf{A}_w)^2 + V_w, \quad (25)$$

where we omitted the scalar potential  $\Phi$ . This is justified since it leads to a negligible modification of the potential  $V_w$ . Equation (25) represents the Hamiltonian of a spinless, charged particle with mass  $\mu$  in a magnetic field  $\mathbf{B}$  and in the potential  $V_w$ . Next we investigate the bound states of  $H_w$  and focus on the 2-dimensional setting where the motion is confined to the  $x-y$  plane. This is justified because the dipole-dipole interaction confines the relative atomic motion to this plane, see Fig. 3(b). We find that Eq. (25) can be written as

$$H_w = \frac{1}{2\mu}\mathbf{p}^2 + V_w + H_Z + H_D, \quad (26)$$

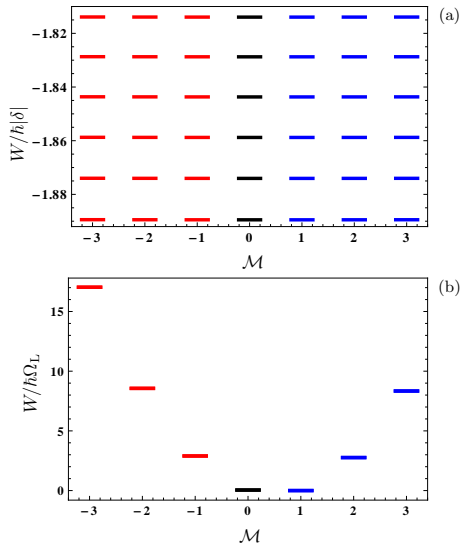


FIG. 4. (Color online) (a) Lowest vibrational states in the potential shown in Fig. 3(a) for  $\Delta = -3|\delta|$  and  $\Omega_L/|\delta| = 2.8 \times 10^{-6}$ . The energy difference of the vibrational states is  $\omega_{\text{vib}} \approx 0.015|\delta|$ . (b) Lowest vibrational state for different quantum numbers  $M$  and on an energy scale defined by  $\hbar\Omega_L$ .

where

$$H_Z = -\frac{1}{\mu} \frac{A_w^{(\phi)}}{\rho} L_z, \quad (27)$$

$$H_D = \frac{[A_w^{(\phi)}]^2}{2\mu}. \quad (28)$$

The operator  $L_z$  in Eq. (27) is the  $z$  component of the orbital angular momentum associated with the relative atomic motion. It follows that  $H_Z$  can be regarded as a Zeeman Hamiltonian (see, e.g., complement DVII in [27]). Note that the pre-factor  $A_w^{(\phi)}/\rho$  in Eq. (27) can be identified with  $B_z$  if  $A_w^{(\phi)}$  did not depend on  $\rho$ . The remaining contribution  $H_D$  in Eq. (28) is the diamagnetic term of the Hamiltonian  $H_w$  (see, e.g., complement DVII in [27]).

Next we show that the Zeeman Hamiltonian lifts the degeneracy between rotational states differing only by the sign of their azimuthal angular momentum. The splitting of Zeeman levels is typically given by the Larmor angular frequency  $\omega_L = qB/(2m)$ , where  $q$  is the charge and  $m$  is the mass of the particle. The corresponding quantity in our case is

$$\omega_L = \frac{\hbar}{2\mu R_0^2} \tilde{B} = \Omega_L \tilde{B}, \quad (29)$$

where  $\tilde{B} = B/(\hbar/R_0^2)$  is the dimensionless magnetic field shown in Fig. 3(b) and

$$\Omega_L = \frac{\hbar}{2\mu R_0^2}. \quad (30)$$

The parameter  $\hbar\Omega$  is the rotational constant of a rigid rotor comprised of two equal particles of mass  $2\mu$  and separated by  $R_0$ . For  $^{39}\text{K}$  atoms with principal quantum number  $n = 30$  and  $|\delta| = 2\pi \times 11.4$  MHz, we obtain  $R_0 = 2.85\mu\text{m}$  and  $\Omega_L \approx 2\pi \times 31.9$  Hz. Larger values can be obtained for lighter atoms and smaller values of  $R_0$ , which corresponds to lower values of the principal quantum number  $n$ . For example, for  $^{23}\text{Na}$  atoms with principal quantum number  $n = 15$  and  $|\delta| = 2\pi \times 39.0$  MHz, we obtain  $R_0 = 0.75\mu\text{m}$  and  $\Omega_L \approx 2\pi \times 780$  Hz [28].

Next we find the spectrum of  $H_w$  by numerical methods. Since  $L_z$  commutes with all other parts of the Hamiltonian, we can find simultaneous eigenstates of  $H_w$  and  $L_z$ . The eigenfunctions of  $L_z$  are  $e^{i\mathcal{M}\phi}$  with integer  $\mathcal{M}$ , and the corresponding eigenvalues are  $\hbar\mathcal{M}$ . Note that the quantum number  $\mathcal{M}$  corresponds to the relative motion of the two Rydberg atoms, and must not be confused with the azimuthal quantum number  $m_j$  associated with the internal Zeeman states. Furthermore, we assume that  $\alpha_w$  is strongly localised in the  $z$  direction. The Ansatz

$$\alpha_w(\rho, z, \phi) \propto e^{i\mathcal{M}\phi} \mathcal{R}(\rho) \mathcal{Z}(z) \quad (31)$$

yields an effective equation for  $\mathcal{R}(\rho)$ , and we find the spectrum of the corresponding Hamiltonian via a discretisation of the spatial variable  $\rho$ . This procedure yields the vibrational energy states in the potential well in Fig. 3(a). The result for the lowest vibrational states in the potential of Fig. 2 for  $\Delta = -3|\delta|$  is shown in Fig. 4(a). We find that the energy difference of the vibrational states is  $\omega_{\text{vib}} \approx 0.015|\delta|$ , which yields  $\omega_{\text{vib}} \approx 2\pi \times 171$  kHz for  $|\delta| = 2\pi \times 11.4$  MHz. Each vibrational state is quasi-degenerate with respect to the quantum number  $\mathcal{M}$  on the energy scale of  $\hbar|\delta|$ . However, Fig. 4(b) shows the lowest vibrational state for different quantum numbers  $\mathcal{M}$  and on an energy scale defined by  $\hbar\Omega_L$ . Here we clearly see the anticipated Zeeman splitting of the magnetic sublevels. The splitting between the  $\mathcal{M} = 2$  and  $\mathcal{M} = 1$  state is approximately given by  $2.76 \times \Omega_L$ . Note that this relation is approximately independent of the ratio  $\Omega_L/|\delta|$ . Since the dipole-dipole interaction is not a central potential, the total orbital angular momentum of the relative motion is not conserved. The kinetic energy term in  $H_w$  contains a term that is quadratic in  $\mathcal{M}$ , and thus the Zeeman spectrum looks different from that of atomic physics.

We emphasise that the ground state of the system is the  $\mathcal{M} = 1$  state [see Fig. 5(b)], although the difference to the  $\mathcal{M} = 0$  state is small. In addition, all  $\mathcal{M} > 0$  states lie below their negative counterparts. In order to provide a physical explanation for this result, we derive from Eq. (25) a dynamical equation for the Heisenberg operator  $\mathbf{R}$ ,

$$\begin{aligned} \mu \partial_t^2 \mathbf{R} = & -\nabla V_w \\ & + \frac{1}{2\mu} \left\{ [(\mathbf{p} - \tilde{\mathbf{A}}) \times \mathbf{B}] - [\mathbf{B} \times (\mathbf{p} - \tilde{\mathbf{A}})] \right\}. \end{aligned} \quad (32)$$

The second line in Eq. (32) describes the Lorentz force given by the vector product of the magnetic field and the velocity  $(\mathbf{p} - \tilde{\mathbf{A}})/\mu$  of the relative motion. Since the magnetic field points downwards near the minimum of the potential well in Fig. 3(a) [see Fig. 3(b)], the Lorentz force favours motion in anti-clockwise direction. This explains why the  $\mathcal{M} > 0$  states have lower energy as compared to their negative counterparts.

The level structure of the bound states inside the potential well influence the quantum dynamics of the system. For example, it gives rise to a geometric phase which could be measured, in principle, via an Aharonov-Bohm type interference experiment [29]. In addition, the deflection of the relative motion via the Lorentz force offers a different route towards the experimental measurement of the effective magnetic field [30].

#### IV. NON-ABELIAN GAUGE FIELDS

The vector potential  $\tilde{\mathbf{A}}$  represents a non-Abelian gauge field if not all of its components  $\tilde{A}^{(k)}$  commute with each other. This situation can only arise if the relative motion induces non-adiabatic transitions between  $q \geq 2$  eigenstates of  $H_{\text{int}}$ . In this case, the components of  $\tilde{\mathbf{A}}$  are  $q \times q$  matrices that do not necessarily commute. Here we focus on the case  $q = 2$  and assume that  $|\psi_1\rangle$  is the well state studied in Sec. III. We find that the corresponding energy curve  $\epsilon_1$  exhibits an avoided crossing with a second well state  $|\psi_2\rangle$ . This is shown in Fig. 5(a), where  $\epsilon_1$  ( $\epsilon_2$ ) is represented by the solid red line (black dashed line). We point out that the two energy curves cross for  $\delta = \Delta$ , and hence the two lines represent a conical intersection [31, 32] with respect to the parameters  $\Delta/|\delta|$  and  $R$ . In the following we evaluate all components of the vector potential  $\tilde{\mathbf{A}}$ , and show that it can induce transitions between the states  $|\psi_1\rangle$  and  $|\psi_2\rangle$ . Furthermore, we demonstrate that  $\tilde{\mathbf{A}}$  is a non-Abelian gauge field. Note that the description of non-adiabatic transitions via gauge fields is a well-established technique in molecules [31, 32]. In addition, it has been applied to dipole-dipole interacting Rydberg atoms in [33–35].

The Hamiltonian for the quantum dynamics of the relative motion and the two internal states can be obtained from Eq. (12) for  $q = 2$ . We find

$$H_2 = \frac{1}{2\mu} \left[ \mathbf{p}^2 \mathbf{1}_2 - 2\tilde{\mathbf{A}} \cdot \mathbf{p} - (\mathbf{p} \cdot \tilde{\mathbf{A}}) + \tilde{\mathbf{A}}^2 \right] + \tilde{V}, \quad (33)$$

where we omitted the scalar potential  $\Phi$  because its impact on the presented results is negligible. All off-diagonal terms of  $H_2$  can give rise to a coupling between the relative atomic motion and the internal electronic states. In order to investigate the coupling terms in Eq. (33) in detail, we evaluate all components of the vector potential  $\tilde{\mathbf{A}}$  as outlined in Appendix B. The result is shown in Figs. 5(b) and (c), where all non-zero components of  $\tilde{A}^{(1)}$  and  $\tilde{A}^{(2)}$  are displayed, respectively. Note

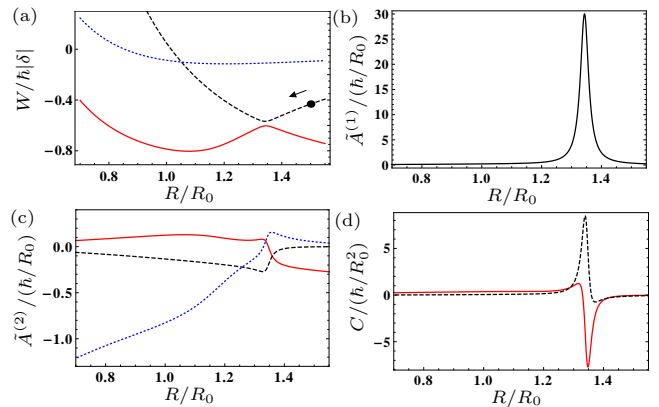


FIG. 5. (Color online) (a) Three potential wells in the  $x - y$  plane corresponding to three different eigenstates of  $H_{\text{int}}$ . The solid red, black dashed, and blue dotted lines correspond to  $|\psi_1\rangle$ ,  $|\psi_2\rangle$ , and  $|\psi_3\rangle$ , respectively. The black dot indicates the initial position of the system for the dynamics discussed in Fig. 6, and the arrow indicates the direction of motion. (b) Imaginary part of  $\tilde{A}_{12}^{(1)} = [\tilde{A}_{21}^{(1)}]^*$  for  $\phi = 0$ . (c) Real parts of  $\tilde{A}_{11}^{(2)}$  (solid red line),  $\tilde{A}_{22}^{(2)}$  (dashed black line) and  $\tilde{A}_{12}^{(2)} = [\tilde{A}_{21}^{(2)}]^*$  (dotted blue line) for  $\phi = 0$ . (d) Matrix elements of the commutator  $C$  in Eq. (34). The red solid line shows  $C_{11} = -C_{22}$ , and the black dashed line represents  $C_{12} = C_{21}$ . In (a)-(d), we set  $\Delta = -1.13|\delta|$ . All components of  $\tilde{\mathbf{A}}$  that are not shown in (b) and (c) are zero.

that we evaluate  $\tilde{\mathbf{A}}$  for  $\phi = 0$  such that  $\tilde{A}^{(1)}$  ( $\tilde{A}^{(2)}$ ) corresponds to the radial (azimuthal) component of  $\tilde{\mathbf{A}}$ . We find that the dominant coupling term in Eq. (33) is proportional to  $\tilde{\mathbf{A}}_{12} \cdot \mathbf{p}$ . Since the largest component of  $\tilde{\mathbf{A}}_{12}$  is  $\tilde{A}_{12}^{(1)}$  [see Figs. 5(b) and (c)], it follows that radial motion gives rise to the strongest coupling between states  $|\psi_1\rangle$  and  $|\psi_2\rangle$ . An estimate shows that the coupling near the avoided crossing can become near-resonant for realistic Rydberg atom parameters.

A quantitative analysis of the coupling between internal states and the relative atomic motion can be obtained from a semi-classical simulation of the system dynamics. To this end we treat the relative motion of the atoms classically, i.e., we derive a set of coupled equations for the mean values  $\langle \mathbf{R} \rangle$  and  $\langle \mathbf{p} \rangle$  from the full Hamiltonian  $H_{\text{int}}$  in Eq. (3). We assume that the dynamics is confined to the  $x - y$  plane. This is justified because the anisotropic dipole-dipole interaction provides a trapping potential in the  $z$  direction. Furthermore, we assume that the system is initially at rest and prepared in state  $|\psi_2\rangle$  at  $\rho = 1.5R_0$ , see Fig. 5(a). This could be realised if the ground state atoms are trapped in optical tweezers [36, 37] and subsequently excited to the Rydberg and molecule levels. The result of the semi-classical simulation of the system dynamics is shown Fig. 6. At the initial position  $\rho = 1.5R_0$  the system experiences the attractive part of the potential curve  $\epsilon_2$ . It thus starts to move towards the avoided crossing at  $\rho \approx 1.33R_0$ , see Figs. 5(a) and 6(a). Near the avoided crossing transitions between the two internal

states occur, and eventually an almost equal superposition of the states  $|\psi_1\rangle$  and  $|\psi_2\rangle$  is created [see Fig. 6(b)].

Note that this semi-classical approach does not account for all physical phenomena. In particular, in a full quantum mechanical treatment the relative motion is described by a wavepacket that splits as it moves across the avoided crossing. The two wavepackets corresponding to the internal states  $|\psi_1\rangle$  and  $|\psi_2\rangle$  experience different potentials and will thus separate in space. It follows that the avoided crossing acts like a beamsplitter for the wavepacket of the relative motion. The full quantum mechanical analysis of this problem is beyond the scope of this work and will be presented elsewhere [30]. The experimental observation of the splitting of the motional wavepacket requires measurements of the density-density correlations of the two Rydberg atoms. Such measurements have been performed by ionization of the Rydberg atoms [25] and by de-excitation to the ground state followed by advanced imaging techniques [38]. We thus believe that the synthetic spin-orbit coupling is detectable with current or next-generation imaging techniques.

The preceding results demonstrate that the vector potential  $\tilde{\mathbf{A}}$  results in a coupling between the relative atomic motion and internal electronic states. It follows that our system realises a synthetic spin-orbit coupling. In addition, we find that all components of the commutator

$$C = \frac{i}{\hbar} [\tilde{A}^{(1)}, \tilde{A}^{(2)}] \quad (34)$$

are different from zero, see Fig. 5(d). It follows that the gauge fields  $A^{(1)}$  and  $A^{(2)}$  are non-Abelian. We point out that the diagonal elements of  $C$  can be calculated directly without the knowledge of the vector potential  $\tilde{\mathbf{A}}$ . This is shown in Appendix C. The non-Abelian character of the gauge fields has a direct impact on the magnetic field via Eqs. (17) and (18). Since the commutator  $C$  is of the same order of magnitude as the artificial magnetic field experienced in state  $|\psi_1\rangle$  alone [see Fig. 3(b)], the non-Abelian effects will be of the same size as the impact of the magnetic field on the quantum dynamics in the internal state  $|\psi_1\rangle$ . In particular, the Lorentz force acting on the relative atomic motion will contain a distinct signature of the non-Abelian character of the gauge fields [39]. A more detailed investigation of non-Abelian signatures [40] in the quantum dynamics of our system is work in progress and will be presented elsewhere.

Finally, we point out that the full dynamics of this system is much richer than the  $U(2)$  gauge theory discussed so far. The blue dotted line in Fig. 5 shows the energy curve  $\epsilon_3$  of a third state  $|\psi_3\rangle$ , which crosses  $|\psi_2\rangle$  at  $R \approx R_0$ . This crossing turns into an avoided crossing outside the  $x - y$  plane, and hence it can be regarded as a conical intersection [31, 32]. For small values of  $z$ , the coupling between  $|\psi_2\rangle$  and  $|\psi_3\rangle$  will be significant, and thus all three states have to be taken into account.

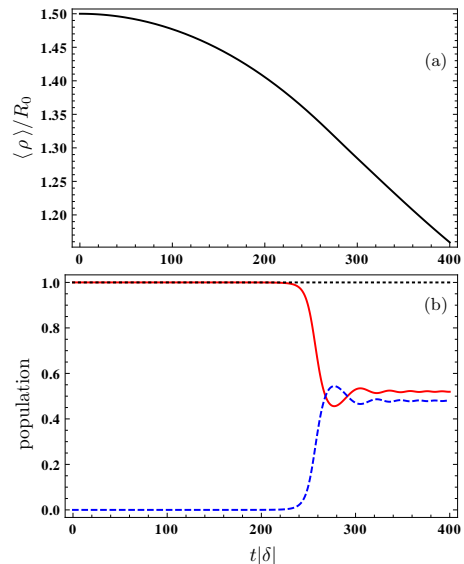


FIG. 6. (Color online) Semi-classical simulation of the system dynamics in the  $x - y$  plane. The initial conditions are  $\langle \rho \rangle = 1.5R_0$  and  $\langle \mathbf{p} \rangle = \mathbf{0}$ . The system is prepared in the internal state  $|\psi_2\rangle$  at  $t = 0$ . The parameters are  $\Delta = -1.13|\delta|$  and  $\Omega_L/|\delta| = 2.8 \times 10^{-6}$ , corresponding to  $|\delta| = 2\pi \times 11.4$  MHz,  $^{39}\text{K}$  atoms with principal quantum number  $n = 30$  and  $R_0 = 2.85\mu\text{m}$ . We neglect effects due to the finite lifetime of the molecule ( $t|\delta| \approx 1300$ ) [41] and thus restrict the analysis to times that are significantly smaller. (a) Position  $\langle \rho \rangle$  as a function of time. (b) Population of the internal states. The red solid line corresponds to  $|\psi_2\rangle$ , and the blue dashed line shows the population in  $|\psi_1\rangle$ . The black dotted line shows the sum of the population in  $|\psi_1\rangle$  and  $|\psi_2\rangle$ .

## V. SUMMARY AND DISCUSSION

In summary, we have shown that the dipole-dipole interaction between Rydberg atoms can induce sizeable Abelian and non-Abelian artificial gauge fields affecting the relative motion of the two atoms. Our system is several orders of magnitude larger than conventional molecules, and the exquisite control over individual Rydberg atoms allows one to engineer non-trivial gauge fields. In the case of an Abelian gauge field and adiabatic motion in a single molecular state, the corresponding magnetic field results in a Zeeman shift of the rotational states. More specifically, the Zeeman shift lifts the degeneracy of rotational states whose azimuthal angular momenta have opposite sign. This result reflects the broken symmetry in our system due to the different Stark shifts of the  $m_j > 0$  and  $m_j < 0$  magnetic sublevels of the individual Rydberg atoms. In particular, we find that the ground state of the potential well is given by the first excited rotational state.

The relative atomic motion can induce transitions between internal two-atom states. This coupling is mediated by off-diagonal terms of the artificial gauge fields. We find that our system exhibits this synthetic spin-orbit coupling near an avoided crossing of two well states. In

addition, we show that the corresponding gauge fields are non-Abelian.

We expect that similar effects arise in other dipole-dipole interacting systems like polar molecules and magnetic atoms. Although the dipole-dipole interaction is much weaker in those systems, they are not limited by the finite lifetime of Rydberg atoms.

### Appendix A: Hamiltonian $H_{\text{int}}$ of the internal states

The dynamics of the internal states is governed by the Hamiltonian  $H_{\text{int}} = H_S + V_{\text{dd}}$ . The Hamiltonian of the electronic levels  $H_S$  is

$$H_S = \hbar \sum_{\mu=1}^2 [(\omega_0 + \delta)|p-1/2\rangle_{\mu}\langle p-1/2|_{\mu} + (\omega_0 + \Delta)|p+1/2\rangle_{\mu}\langle p+1/2|_{\mu} + \omega_0(|p+3/2\rangle_{\mu}\langle p+3/2|_{\mu} + |p-3/2\rangle_{\mu}\langle p-3/2|_{\mu})]. \quad (\text{A1})$$

Here  $\omega_0$  is the resonance frequency of the  $|s \pm 1/2\rangle \leftrightarrow |p \pm 3/2\rangle$  transition.

The symmetric level scheme with  $\Delta = \delta$  can be realized if a static electric field is applied in  $z$  direction [23]. The asymmetry  $\Delta \neq \delta$  could be induced, e.g., by the application of an additional  $\sigma^+$  polarized AC field inducing AC Stark shifts [42, 43] of the  $|s-1/2\rangle \leftrightarrow |p+1/2\rangle$  and  $|s+1/2\rangle \leftrightarrow |p+3/2\rangle$  transitions. Since the Clebsch-Gordan coefficients on these transitions are different, these Stark shifts change the energy difference between the  $|p+1/2\rangle$  and  $|p+3/2\rangle$  states and thus result in  $\Delta \neq \delta$ . In addition, the AC Stark shifts will lift the degeneracy of the  $|p \pm 3/2\rangle$  and  $|s \pm 1/2\rangle$  states. However, as shown in Sec. III any level scheme where states with positive and negative azimuthal quantum numbers have different energies results in an effective magnetic field. We have verified explicitly that non-degenerate  $|p \pm 3/2\rangle$  states result in qualitatively similar results as compared to the level scheme in Fig. 1(a).

The dipole-dipole interaction is given by [44]

$$V_{\text{dd}} = \frac{1}{4\pi\epsilon_0 R^3} [\hat{\mathbf{d}}^{(1)} \cdot \hat{\mathbf{d}}^{(2)} - 3(\hat{\mathbf{d}}^{(1)} \cdot \vec{\mathbf{R}})(\hat{\mathbf{d}}^{(2)} \cdot \vec{\mathbf{R}})], \quad (\text{A2})$$

where  $\hat{\mathbf{d}}^{(i)}$  is the electric dipole-moment operator of atom  $i$  and  $\vec{\mathbf{R}} = \mathbf{R}/R$  is the unit vector along the molecular axis. For the evaluation of Eq. (A2) we compute the matrix elements of the dipole operator via the Wigner-Eckart theorem [45] according to

$$\langle pm|\hat{\mathbf{d}}^{(i)}|sm'\rangle = \underbrace{\frac{(np_{3/2}\|\hat{\mathbf{d}}\|ns_{1/2})}{[2 \cdot 3/2 + 1]^{1/2}}}_{=\mathcal{D}} \sum_{q=-1}^1 C_{1/2m'1q}^{3/2m} \vec{\epsilon}_q, \quad (\text{A3})$$

where  $C_{1/2m'1q}^{3/2m}$  are Clebsch-Gordan coefficients and  $\vec{\epsilon}_q$  are orthonormal unit vectors arising from the decomposition of the dipole operator into its spherical components [45]. The reduced matrix element  $(np_{3/2}\|\hat{\mathbf{d}}\|ns_{1/2})$  in Eq. (A3) can be written in terms of a radial matrix element between the  $np_{3/2}$  and  $ns_{1/2}$  states [23, 45–47]. Since the sum in Eq. (A3) is a term of order unity, the magnitude of  $V_{\text{dd}}$  is given by

$$\hbar\Omega = |\mathcal{D}|^2/(4\pi\epsilon_0 R^3). \quad (\text{A4})$$

Equating  $\Omega$  to  $|\delta|$  yields the characteristic length  $R_0$ , given by

$$R_0 = (|\mathcal{D}|^2/(4\pi\epsilon_0\hbar|\delta|))^{1/3}. \quad (\text{A5})$$

We scale all energies with the Stark shift  $\hbar|\delta|$ , and thus  $V_{\text{dd}}$  only depends on the ratio  $R/R_0$ . In the subspace of  $nsnp$  states, the frequency  $\omega_0$  appears as an offset to all states and can thus be eliminated. Scaling  $H_S$  with  $\hbar|\delta|$  leaves the ratio  $\Delta/\delta$  as the only remaining free parameter.

### Appendix B: Evaluation of the vector potential $\mathbf{A}$

The off-diagonal elements of the vector potential are given by [48]

$$\mathbf{A}_{kl} = \frac{i\hbar}{\epsilon_l - \epsilon_k} \langle \psi_k(\mathbf{R}) | [\nabla H_{\text{int}}(\mathbf{R})] | \psi_l(\mathbf{R}) \rangle. \quad (\text{B1})$$

Note that Eq. (B1) can be evaluated without any phase convention for the eigenstates  $|\psi_l(\mathbf{R})\rangle$ , i.e., via the numerical diagonalisation of  $H_{\text{int}}$ . On the other hand, Eq. (B1) will only yield continuous expressions for  $\mathbf{A}_{kl}(\mathbf{R})$  as a function of  $\mathbf{R}$  if a suitable phase convention for the eigenstates  $|\psi_l(\mathbf{R})\rangle$  is imposed. In the following, we employ a particular phase convention that allows us to evaluate the diagonal elements of  $\mathbf{A}$  as well.

We first explain our phase convention for states in a plane with constant  $\phi$ . Without loss of generality we consider the plane with  $\phi = 0$  and pick one reference point  $\mathbf{R}_0$ . In order to fix the phase of an eigenstate  $|\psi_n(\mathbf{P})\rangle$  at  $\mathbf{P}$  we impose the condition of parallel transport, i.e.,

$$\langle \psi_n(\mathbf{R}) | \nabla | \psi_n(\mathbf{R}) \rangle \cdot \mathbf{e}_{\mathbf{R}_0\mathbf{P}} = 0, \quad (\text{B2})$$

where the unit vector  $\mathbf{e}_{\mathbf{R}_0\mathbf{P}}$  points from  $\mathbf{R}_0$  to  $\mathbf{P}$  and  $\mathbf{R}$  is an arbitrary point on the straight line connecting  $\mathbf{R}_0$  and  $\mathbf{P}$ . In the absence of degeneracies, this means that we obtain  $|\psi_n(\mathbf{P})\rangle$  by adiabatic evolution from  $|\psi_n(\mathbf{R}_0)\rangle$ . In general, the condition (B2) does not guarantee that the phase of  $|\psi_n(\mathbf{R})\rangle$  is a smooth function of position. If one considers adiabatic evolution on a closed path in the  $\phi = 0$  plane, the state will acquire a Berry phase that is equal to the magnetic flux enclosed by the circular path. However, the nature of the dipole-dipole interaction cannot create a magnetic flux in  $\mathbf{e}_{\phi}$  direction, and thus Eq. (B2) leads to a well-defined phase as a function of position.



In order to put this line of thought on formal grounds, we prove that the magnetic field component  $B_n^{(\phi)}$  is indeed zero for every state  $|\psi_n\rangle$ . With Eq. (C8) we find

$$\begin{aligned} [(\nabla \times \mathbf{A}_n) \cdot \mathbf{e}_\phi]_{\phi=0} &= (\partial_3 A_n^{(1)} - \partial_1 A_n^{(3)})_{\phi=0} \quad (\text{B3}) \\ &= \frac{i}{\hbar} \sum_{p \neq n} \left( A_{np}^{(3)} A_{pn}^{(1)} - A_{np}^{(1)} A_{pn}^{(3)} \right)_{\phi=0} \\ &= \frac{i}{\hbar} \sum_{p \neq n} 2i \operatorname{Im} \left( A_{np}^{(3)} A_{pn}^{(1)} \right)_{\phi=0}. \end{aligned}$$

Equation (B1) allows us to write

$$A_{np}^{(3)} A_{pn}^{(1)} = \frac{\hbar^2}{(\epsilon_p - \epsilon_n)^2} \langle \psi_n | [\partial_3 H_{\text{int}}] | \psi_p \rangle \langle \psi_p | [\partial_1 H_{\text{int}}] | \psi_n \rangle. \quad (\text{B4})$$

We find that  $\partial_3 H_{\text{int}}$ ,  $\partial_1 H_{\text{int}}$  and  $H_{\text{int}}$  are real and symmetric matrices for  $\phi = 0$ . In particular, since  $H_{\text{int}}$  is real and symmetric, all components of the eigenstates  $|\psi_n\rangle$  in the Zeeman basis are real [up to an overall complex factor, which drops out in Eq. (B4)]. It follows that the expression in Eq. (B4) is real, and thus we have

$$[(\nabla \times \mathbf{A}_n) \cdot \mathbf{e}_\phi]_{\phi=0} = \partial_z A_n^{(\rho)} - \partial_r A_n^{(z)} = 0. \quad (\text{B5})$$

This implies that there exists a function  $S_n(\rho, z)$  such that  $\partial_\rho S_n = A_n^{(\rho)}$  and  $\partial_z S_n = A_n^{(z)}$ . Condition (B2) means that the line integral of  $\mathbf{A}_n$  from  $\mathbf{R}_0$  to  $\mathbf{P}$  is zero, and hence  $S_n$  is constant throughout the  $\phi = 0$  plane. It follows that

$$\partial_\rho S_n = A_n^{(\rho)} = \langle \psi_n(\mathbf{R}) | \nabla | \psi_n(\mathbf{R}) \rangle \cdot \mathbf{e}_\rho = 0, \quad (\text{B6})$$

$$\partial_z S_n = A_n^{(z)} = \langle \psi_n(\mathbf{R}) | \nabla | \psi_n(\mathbf{R}) \rangle \cdot \mathbf{e}_z = 0 \quad (\text{B7})$$

at every point in the  $\phi = 0$  plane.

Since the system exhibits azimuthal symmetry, all states at  $\mathbf{R}$  outside the plane with  $\phi = 0$  can be generated from those in the plane via a unitary rotation operator [49],

$$|\psi_n(\rho, z, \phi)\rangle = e^{-i/\hbar J_z \phi} |\psi_n(\rho, z, \phi = 0)\rangle, \quad (\text{B8})$$

where  $J_z = J_z^{(1)} + J_z^{(2)}$  and  $J_z^{(\mu)}$  is the  $z$  component of the total angular momentum operator of the internal states of atom  $\mu$ . It follows from Eq. (B8) that relations (B6) and (B7) hold for any  $\mathbf{R}$ , and the only non-zero component of  $\mathbf{A}_n$  is given by

$$A_n^{(\phi)}(\rho, z) = i\hbar \langle \psi_n(\mathbf{R}) | \nabla | \psi_n(\mathbf{R}) \rangle \cdot \mathbf{e}_\phi \quad (\text{B9})$$

$$= i\hbar \frac{1}{\rho} \langle \psi_n(\mathbf{R}) | \partial_\phi | \psi_n(\mathbf{R}) \rangle. \quad (\text{B10})$$

According to Eq. (B8),  $A_n^{(\phi)}(\rho, z)$  is proportional to the mean value of the operator  $J_z$ ,

$$A_n^{(\phi)}(\rho, z) = \frac{1}{\rho} \langle \psi_n(\mathbf{R}) | J_z | \psi_n(\mathbf{R}) \rangle. \quad (\text{B11})$$

This result allows us to evaluate the diagonal elements of  $\mathbf{A}_n$  by numerical means.

### Appendix C: Evaluation of the curvature

The Berry curvature in Eq. (19) can be written as

$$\Omega_{nm}^{(kl)} = i\hbar (\langle \partial_k \psi_n | \partial_l \psi_m \rangle - \langle \partial_l \psi_n | \partial_k \psi_m \rangle) \quad (\text{C1})$$

$$= \frac{i}{\hbar} \sum_{p=1}^N \left( A_{np}^{(k)} A_{pm}^{(l)} - A_{np}^{(l)} A_{pm}^{(k)} \right) \quad (\text{C2})$$

$$= \frac{i}{\hbar} \left[ A^{(k)}, A^{(l)} \right]_{nm}, \quad (\text{C3})$$

where we employed Eq. (B1). We point out that Eqs. (18) and (C3) imply that the magnetic field is equal to zero if all  $N$  states comprise the system of interest, i.e., if  $q = N$ . If the system of interest consists of the first  $q$  states, we have

$$F_{nm}^{(kl)} = \Omega_{nm}^{(kl)} - \frac{i}{\hbar} \left[ \tilde{A}^{(k)}, \tilde{A}^{(l)} \right]_{nm}, \quad (\text{C4})$$

where  $n, m \leq q$  and  $\tilde{A}^{(k)}$  is a  $q \times q$  matrix. The commutator on the right hand side of the latter equation can be written as

$$\frac{i}{\hbar} \left[ \tilde{A}^{(k)}, \tilde{A}^{(l)} \right]_{nm} = \frac{i}{\hbar} \sum_{p=1}^q \left( A_{np}^{(k)} A_{pm}^{(l)} - A_{np}^{(l)} A_{pm}^{(k)} \right), \quad (\text{C5})$$

and thus Eq. (C2) yields

$$F_{nm}^{(kl)} = \frac{i}{\hbar} \sum_{p>q}^N \left( A_{np}^{(k)} A_{pm}^{(l)} - A_{np}^{(l)} A_{pm}^{(k)} \right). \quad (\text{C6})$$

Since Eq. (C6) contains only non-diagonal elements of  $\mathbf{A}$ , it can be evaluated via the result in Eq. (B1). Moreover, we emphasise that all diagonal elements of  $F_{nn}^{(kl)} = F_n^{(kl)}$  are completely independent of the phase of the eigenstates. It follows that the diagonal elements of  $\mathbf{B}$  can be calculated via the numerical diagonalisation of  $H_{\text{int}}$ . In particular, for  $q = 1$  we have

$$F_1^{(kl)} = \Omega_1^{(kl)} = \frac{i}{\hbar} \sum_{p>1} \left( A_{1p}^{(k)} A_{p1}^{(l)} - A_{1p}^{(l)} A_{p1}^{(k)} \right). \quad (\text{C7})$$

Note that the latter equation holds for any of the internal states if we re-arrange their order. More generally, we thus have

$$F_n^{(kl)} = \Omega_n^{(kl)} = \frac{i}{\hbar} \sum_{p \neq n} \left( A_{np}^{(k)} A_{pn}^{(l)} - A_{np}^{(l)} A_{pn}^{(k)} \right). \quad (\text{C8})$$

Finally, we demonstrate that the above results can be employed for the (numerical) evaluation of the diagonal elements of the commutator  $[\tilde{A}^{(k)}, \tilde{A}^{(l)}]$ . We have

$$F_n^{(kl)} = \Omega_n^{(kl)} \quad \text{for } q = 1. \quad (\text{C9})$$

$$F_n^{(kl)} = \Omega_n^{(kl)} - \frac{i}{\hbar} \left[ \tilde{A}^{(k)}, \tilde{A}^{(l)} \right]_{nn} \quad \text{for } q > 1. \quad (\text{C10})$$

Subtraction of Eq. (C10) from (C9) yields

$$\frac{\imath}{\hbar} \left[ \tilde{A}^{(k)}, \tilde{A}^{(l)} \right]_{nn} = F_n^{(kl)}(q=1) - F_n^{(kl)}(q>1) \quad (\text{C11})$$

Since  $F_n^{(kl)}(q=1)$  and  $F_n^{(kl)}(q>1)$  can be evaluated numerically without any phase convention for the eigen-

states, the same is true for the diagonal elements of the commutator  $[\tilde{A}^{(k)}, \tilde{A}^{(l)}]$ .

- 
- [1] F. Wilczek and A. Zee, Phys. Rev. Lett. **52**, 2111 (1984)
- [2] J. Moody, A. Shapere, and F. Wilczek, Phys. Rev. Lett. **56**, 893 (1986)
- [3] M. Born and J. R. Oppenheimer, Annalen der Physik **389**, 457 (1927)
- [4] J. Ruseckas, G. Juzeliūnas, P. Öhberg, and M. Fleischhauer, Phys. Rev. Lett. **95**, 010404 (2005)
- [5] J. Dalibard, F. Gerbier, G. Juzeliūnas, and P. Öhberg, Rev. Mod. Phys. **83**, 1523 (2011)
- [6] R. Dum and M. Olshanii, Phys. Rev. Lett. **76**, 1788 (1996)
- [7] Y.-J. Lin, R. L. Compton, A. R. Perry, W. D. Phillips, J. V. Porto, and I. B. Spielman, Phys. Rev. Lett. **102**, 130401 (2009)
- [8] Y.-J. Lin, R. L. Compton, K. Jiménez-García, J. V. Porto, and I. B. Spielman, Nature **462**, 628 (2009)
- [9] Y.-J. Lin, R. L. Compton, K. Jiménez-García, W. D. Phillips, J. V. Porto, and I. B. Spielman, Nat. Phys. **7**, 531 (2011)
- [10] M. Aidelsburger, M. Atala, S. Nascimbène, S. Trotzky, Y.-A. Chen, and I. Bloch, Phys. Rev. Lett. **107**, 255301 (2011)
- [11] D. Jaksch and P. Zoller, New. J. Phys. **5**, 56 (2003)
- [12] J. Struck, C. Ölschläger, R. L. Targat, P. Soltan-Panahi, A. Eckardt, M. Lewenstein, P. Windpassinger, and K. Sengstock, Science **333**, 996 (2011)
- [13] J. Struck, C. Ölschläger, M. Weinberg, P. Hauke, J. Simonet, A. Eckardt, M. Lewenstein, K. Sengstock, and P. Windpassinger, Phys. Rev. Lett. **108**, 225304 (2012)
- [14] K. Jiménez-García, L. J. LeBlanc, R. A. Williams, M. C. Beeler, A. R. Perry, and I. B. Spielman, Phys. Rev. Lett. **108**, 225303 (2012)
- [15] P. Hauke, O. Tieleman, A. Celi, C. Ölschläger, J. Simonet, J. Struck, M. Weinberg, P. Windpassinger, K. Sengstock, M. Lewenstein, and A. Eckardt, Phys. Rev. Lett. **109**, 145301 (2012)
- [16] T. F. Gallagher, *Rydberg Atoms* (Cambridge University Press, Cambridge, 1994)
- [17] J. D. Pritchard, K. J. Weatherill, and C. S. Adams, arXiv:1205.4890
- [18] M. Saffman, T. G. Walker, and K. Molmer, Rev. Mod. Phys. **82**, 2313 (2010)
- [19] C. H. Greene, A. S. Dickinson, and H. R. Sadeghpour, Phys. Rev. Lett. **85**, 2458 (2000)
- [20] V. Bendkowsky, B. Butscher, J. N. J. P. Shaffer, R. Löw, and T. Pfau, Nature **458**, 1005 (2009)
- [21] C. Boisseau, I. Simbotin, and R. Cotè, Phys. Rev. Lett. **88**, 133004 (2002)
- [22] N. Samboy, J. Stanojevic, and R. Cote, Phys. Rev. A **83**, 050501(R) (2011)
- [23] M. Kiffner, H. Park, W. Li, and T. F. Gallagher, Phys. Rev. A **86**, 031401(R) (2012)
- [24] K. R. Overstreet, A. Schwettmann, J. Tallant, D. Booth, and J. P. Shaffer, Nat. Phys. **5**, 581 (2009)
- [25] A. Schwarzkopf, R. E. Sapiro, and G. Raithel, Phys. Rev. Lett. **107**, 103001 (2011)
- [26] M. Kiffner, J. Evers, and C. H. Keitel, Phys. Rev. A **75**, 032313 (2007)
- [27] C. Cohen-Tannoudji, B. Diu, and F. Laloë, *Quantum Mechanics (Volume I)* (J. Wiley & Sons, London, 1977)
- [28] Note that  $|\delta|$  must be much smaller than the  $np$  fine-structure splitting  $\omega_{\text{FS}}$  [23]. Throughout this paper we choose  $50|\delta| \leq \omega_{\text{FS}}$ .
- [29] Y. Aharonov and D. Bohm, Phys. Rev. **115**, 485 (1959)
- [30] M. Kiffner, W. Li and D. Jaksch, *in preparation*.
- [31] D. R. Yarkony, Rev. Mod. Phys. **68**, 985 (1996)
- [32] *Electronic Structure, Dynamics and Spectroscopy*, Vol. **15**, edited by W. Domcke, D. R. Yarkony, and H. Köppel (World Scientific, 2004).
- [33] S. Wüster, C. Ates, A. Eisfeld, and J. M. Rost, Phys. Rev. Lett. **105**, 053004 (2010)
- [34] S. Möbius, S. Wüster, C. Ates, A. Eisfeld, and J. M. Rost, J. Phys. B **44**, 184011 (2011)
- [35] S. Wüster, A. Eisfeld, and J. M. Rost, Phys. Rev. Lett. **106**, 153002 (2011)
- [36] A. Gaëtan, Y. Miroshnychenko, T. W. an A. Chotia, M. Viteau, D. Comparat, P. Pillet, A. Browaeys, and P. Grangier, Nat. Phys. **5**, 115 (2009)
- [37] E. Urban, T. A. Johnson, T. Henage, L. Isenhower, D. D. Yavuz, T. G. Walker, and M. Saffman, Nat. Phys. **5**, 110 (2009)
- [38] P. Schauß, M. Cheneau, M. Endres, T. Fukuhara, S. Hild, A. Omran, T. Pohl, C. Gross, S. Kuhr, and I. Bloch, Nature **491**, 87 (2012)
- [39] B. Zygelman, Phys. Rev. Lett. **64**, 256 (1990)
- [40] A. Jacob, P. Öhberg, G. Juzeliūnas, and L. Santos, Appl. Phys. B **89**, 439 (2007)
- [41] The lifetime of a Rydberg dimer with  $n = 40$  was estimated in [23] to be  $42 \mu\text{s}$  for alkali atoms. Since the lifetime scales with  $n^3$ , we find  $t|\delta| \approx 1300$  for  $|\delta| = 2\pi \times 11.4 \text{ MHz}$  and  $n = 30$ .
- [42] M. L. Zimmerman, M. G. Littman, M. M. Kash, and D. Kleppner, Phys. Rev. A **20**, 2251 (1979)
- [43] P. Bohlouli-Zanjani, J. A. Petrus, and J. D. D. Martin, Phys. Rev. Lett. **98**, 203005 (2007)
- [44] C. Cohen-Tannoudji, J. Dupont-Roc, and G. Grynberg, *Atom-Photon Interactions* (J. Wiley & Sons, 1998)
- [45] A. R. Edmonds, *Angular Momentum in Quantum Mechanics* (Princeton University Press, Princeton, 1960)
- [46] H. Park, P. J. Tanner, B. J. Claessens, E. S. Shuman, and T. F. Gallagher, Phys. Rev. A **84**, 022704 (2011)
- [47] T. G. Walker and M. Saffman, Phys. Rev. A **77**, 032723 (2008)

- [48] D. Xiao, M.-C. Chang, and Q. Niu, *Rev. Mod. Phys.* **82**, 1959 (2010)
- [49] M. Kiffner, J. Evers, and C. H. Keitel, *Phys. Rev. A* **76**, 013807 (2007)